

# Cool-roof effects on thermal and wind environments during heat waves: A case modeling study in Seoul, South Korea



Jong-Jin Baik <sup>a,\*</sup>, Hyejin Lim <sup>a</sup>, Beom-Soon Han <sup>b</sup>, Han-Gyul Jin <sup>a</sup>

<sup>a</sup> School of Earth and Environmental Sciences, Seoul National University, Seoul, 08826, South Korea

<sup>b</sup> Department of Biological and Environmental Engineering, Semyung University, Jecheon, Chungcheongbuk-do, 27136, South Korea

## ARTICLE INFO

### Keywords:

Cool roof  
Heat wave  
Thermal environment  
Wind environment  
WRF model  
Seoul

## ABSTRACT

This study examines cool-roof effects on thermal and wind environments in Seoul, South Korea during the 2018 heat wave through Weather Research and Forecasting (WRF) model simulations. Two 37-day simulations, one with cool roofs that have a higher albedo and the other with conventional roofs, are conducted. In the daytime, cool roofs decrease the 2-m temperature, 10-m wind speed, surface sensible and latent heat fluxes, and planetary boundary layer height but increase the 2-m water vapor mixing ratio. The daytime maximum decreases are 1.0 °C in 2-m temperature and 0.5 m s<sup>-1</sup> in 10-m wind speed. The cool roof-induced reduction of near-surface temperature tends to decrease with increasing heat wave intensity. The decrease in near-surface temperature weakens convergence of near-surface wind, indicating the weakening of daytime urban breeze. Also, the decrease in near-surface temperature, thus decreased land-sea air temperature difference, leads to the weakening of sea breeze. Interestingly, there are occasions on which the cool-roof case produces higher near-surface temperature at late afternoon times in a region of Seoul than the conventional-roof case. This can occur when the cooling caused by the sea breeze in the conventional-roof case is dominant over the cooling due to cool roofs in the cool-roof case.

## 1. Introduction

The heat wave is an atmospheric phenomenon characterized by abnormally and uncomfortably hot weather that lasts at least one day (Geer, 1996), and it can cause devastating impacts on human health, ecosystem, and economy (Easterling et al., 2000; Kovats and Hajat, 2008). In 2010, an extreme heat wave occurred in eastern Europe and Russia and approximately 55,000 people died and at least one million hectares of land burned (Barriopedro et al., 2011). In 2018, South Korea experienced an extreme heat wave. It was the longest-lasting heat wave on record in South Korea, bringing about the largest number of patients suffering from heat-related illnesses and the record-breaking power demand during peak hours (KMA, 2018). Detailed analyses of the 2018 heat wave are given in Ha et al. (2020) and Lee et al. (2020). It is projected that more frequent, more intense, and longer-lasting heat waves will occur as global warming continues (Meehl and Tebaldi, 2004; Cowan et al., 2014).

Overwhelming heat from the heat wave can synergistically interact with the urban heat island (Li and Bou-Zeid, 2013), further deteriorating thermal environment in cities. To make urban environment thermally comfortable and/or reduce damages from heat waves and urban heat islands, strategies for lowering the urban air temperature and their evaluations are needed. Various mitigation

\* Corresponding author.

E-mail address: [jjbaik@snu.ac.kr](mailto:jjbaik@snu.ac.kr) (J.-J. Baik).

strategies have been proposed and evaluated (Coutts et al., 2013; Taleghani, 2018; Balany et al., 2020). These include green roofs, cool roofs, parks, and wind roads. Among them, cool roofs mitigate urban heat islands by increasing roof albedo and thus reflecting more solar radiation. An example of cool roofs is white-painted roofs. White roofs have received much attention as an efficient strategy to mitigate urban heat islands not only because of their substantial cooling effects, but also in consideration of the cost and ease of applying.

Mesoscale numerical modeling studies have been performed to examine the effects of cool roofs on air temperature, wind, and air quality. Santamouris (2014) reviewed strategies for cooling cities and gathered the data from numerical modeling studies around the world, finding that the urban air temperature is expected to decrease by  $0.3^{\circ}\text{C}$  per every 0.1 increase in roof albedo. Cao et al. (2015) showed that in Guangzhou, China, cool roofs reduce average urban midday temperature by  $1.2^{\circ}\text{C}$  for strong heat wave events and by

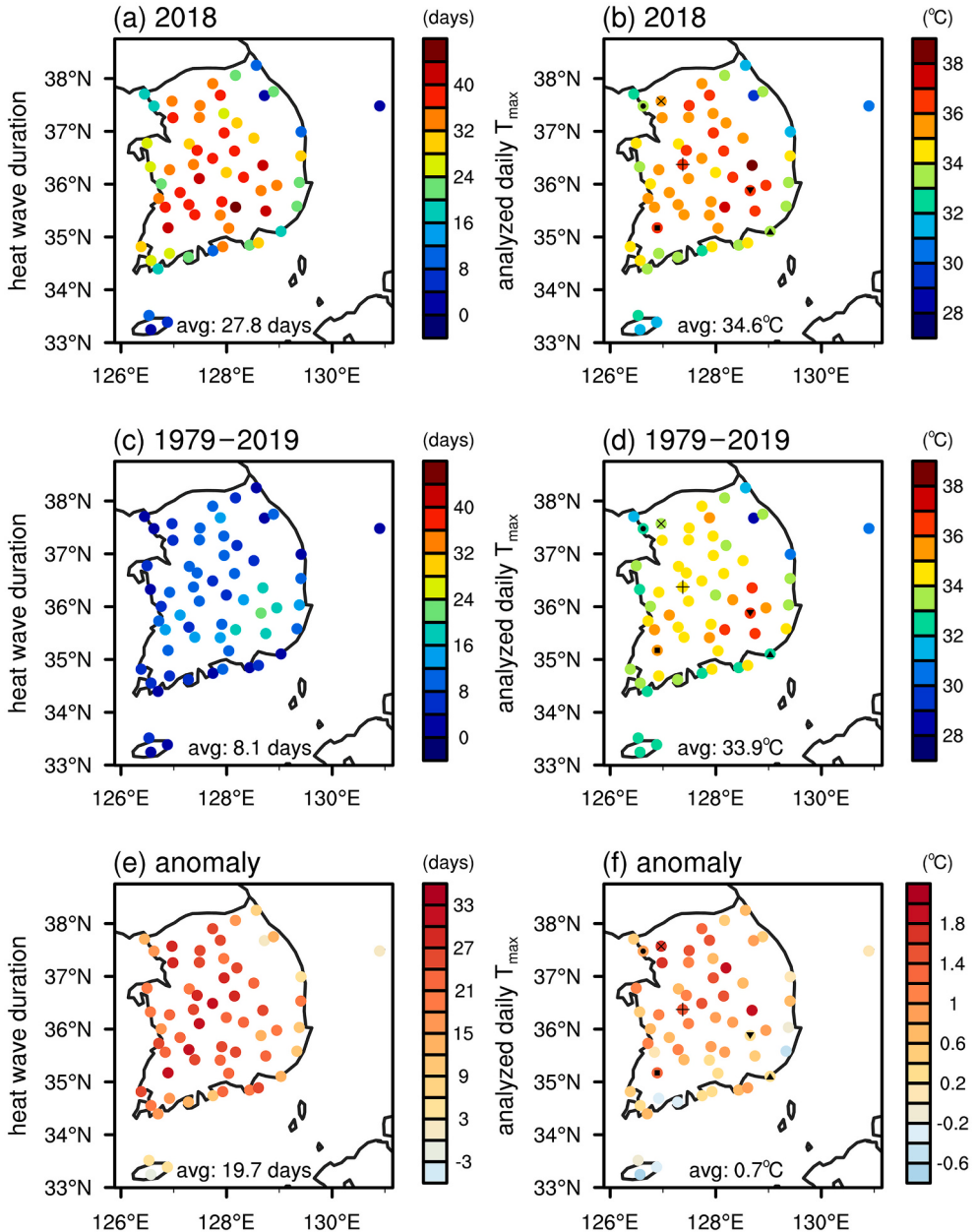


**Fig. 1.** (a, c) Heat wave duration and (b, d) average analyzed daily maximum temperature for 2018 (top row) and 1979–2019 (middle row). The analyzed daily maximum temperature is the daily maximum temperature averaged over the days when the daily maximum temperature averaged over the 60 observatories exceeds  $33^{\circ}\text{C}$ . Anomalies of (e) heat wave duration and (f) average analyzed daily maximum temperature in 2018 from the climatological values for 1979–2019 at each meteorological observatory. In (b, d, f), the six largest cities Seoul, Incheon, Daejeon, Daegu, Gwangju, and Busan are indicated by  $\times$ , ●, +, ▼, ■, and ▲ markers.

0.8 °C for typical summer weeks. [Sharma et al. \(2016\)](#) demonstrated that in Chicago, USA, cool roofs mitigate urban heat islands, modify the structure of the planetary boundary layer, and influence the interaction between lake breeze and urban heat island. [Imran et al. \(2018\)](#) simulated an extreme heatwave event in Melbourne, Australia to evaluate the effects of cool roofs and green roofs and showed that cool roofs have a greater effect on mitigating urban heat islands than green roofs. [Chen and Zhang \(2018\)](#) showed that in the Suzhou–Wuxi–Changzhou metropolitan area, China, the decrease in urban air temperature by cool roofs results in a weakening of daytime lake breeze from a nearby lake. Using a coupled meteorology-air quality modeling system, [Han et al. \(2020\)](#) showed that cool roofs lower near-surface ozone concentration in Seoul, South Korea. It is worth mentioning that the effects of cool roofs on urban air temperature were also examined using a global climate model that has a much coarser horizontal resolution than mesoscale models ([Oleson et al., 2010](#)). Their results indicate that the annual mean urban heat island is decreased by 33% due to cool roofs when averaged over all urban areas.

Previous mesoscale numerical modeling studies (e.g., [Sharma et al., 2016](#); [Chen and Zhang, 2018](#)) suggests that reductions of urban air temperature and changes in local winds due to cool roofs differ depending on geographical locations of cities and meteorological conditions. It would be interesting to investigate the magnitude and horizontal extent of cool-roof effects on near-surface air temperature and wind for Seoul, a megacity adjacent to a sea, during an extreme heat wave using a mesoscale numerical model. In our focus area, local winds such as urban breeze, sea breeze, and mountain wind occur. Cool-roof effects can vary spatially and temporally according to the evolutions of the local winds and their interactions.

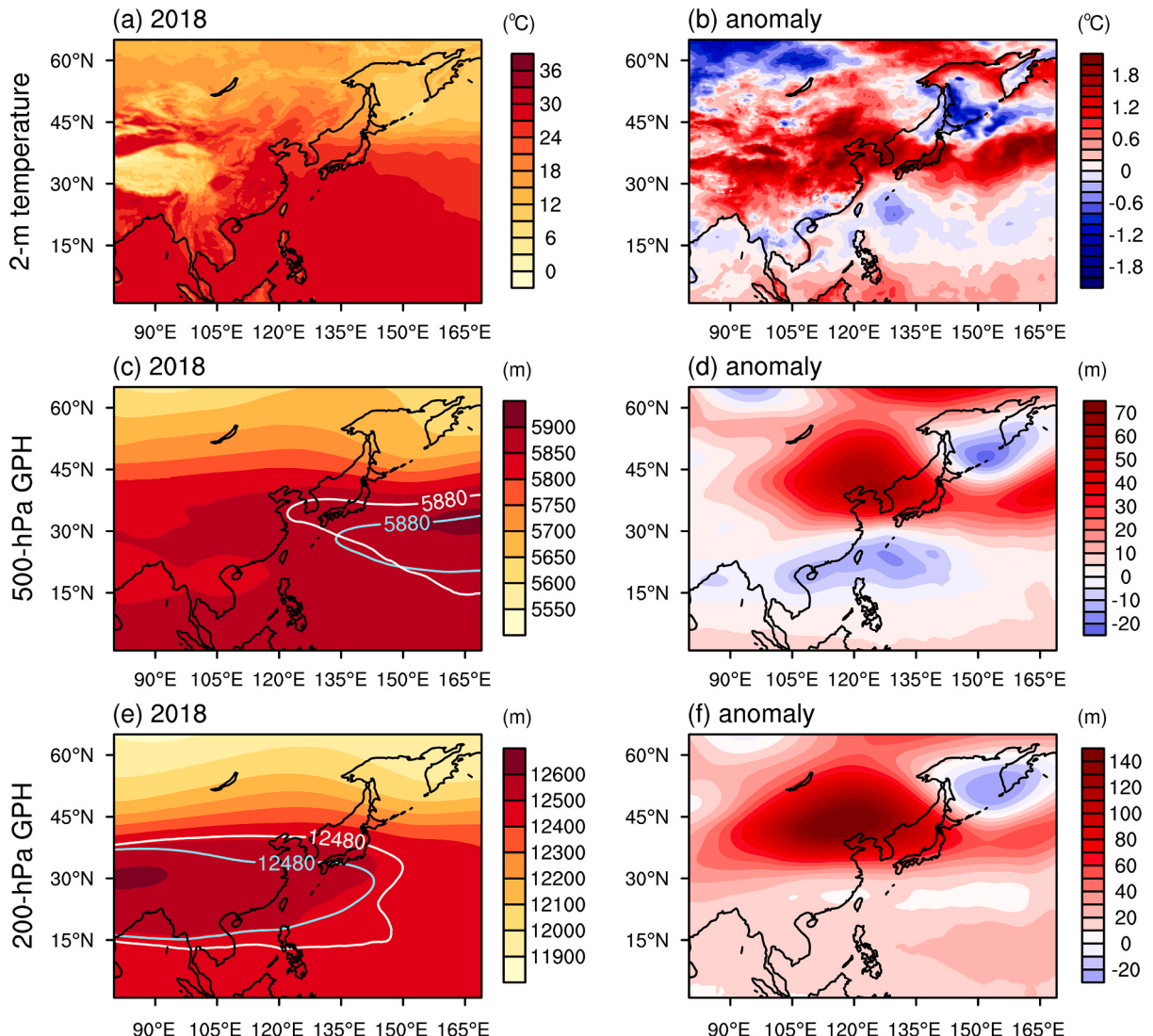


**Fig. 2.** Fields of (a) 2-m temperature and (c) 500- and (e) 200-hPa geopotential heights averaged over July–August 2018. (b), (d), and (f) are their respective anomalies from July–August 1979–2019 climatology. Geopotential height contours of 5880 m and 12,480 m for 2018 (white solid lines) and 1979–2019 (blue solid lines) are drawn in (c) and (e), respectively.

In this study, we examine cool-roof effects on thermal and wind environments in Seoul during the 2018 heat wave through long-term mesoscale numerical model simulations. Section 2 presents features of the 2018 heat wave in brief. Section 3 describes the numerical model and the simulation setup. In section 4, the model is validated and simulation results are presented and discussed. A summary and conclusions are given in section 5.

## 2. Features of the 2018 heat wave

First, the duration and intensity of the 2018 heat wave in South Korea are examined using data from 60 meteorological observatories. South Korea experiences heat waves mostly in July and August, and the daily maximum temperature averaged over these months in 1979–2019 and over all the observatories is 29.2 °C. In this study, the heat wave day is defined as the day when the daily maximum temperature exceeds 33 °C for two or more consecutive days, following the definition used by the Korea Meteorological Administration (KMA). The heat wave duration is the total number of heat wave days. In this study, the analyzed daily maximum temperature is defined at each meteorological observatory as the daily maximum temperature averaged over the days when the daily maximum temperature averaged over the entire 60 meteorological observatories exceeds 33 °C.

Fig. 1 shows the spatial distributions of heat wave duration and analyzed daily maximum temperature for 2018 and 1979–2019, together with their anomalies. A total of 19,982 heat wave days are detected from the 60 meteorological observatories for the period from 1979 to 2019, and July and August occupies 95% of the total. The heat wave duration averaged over all the observatories in 2018

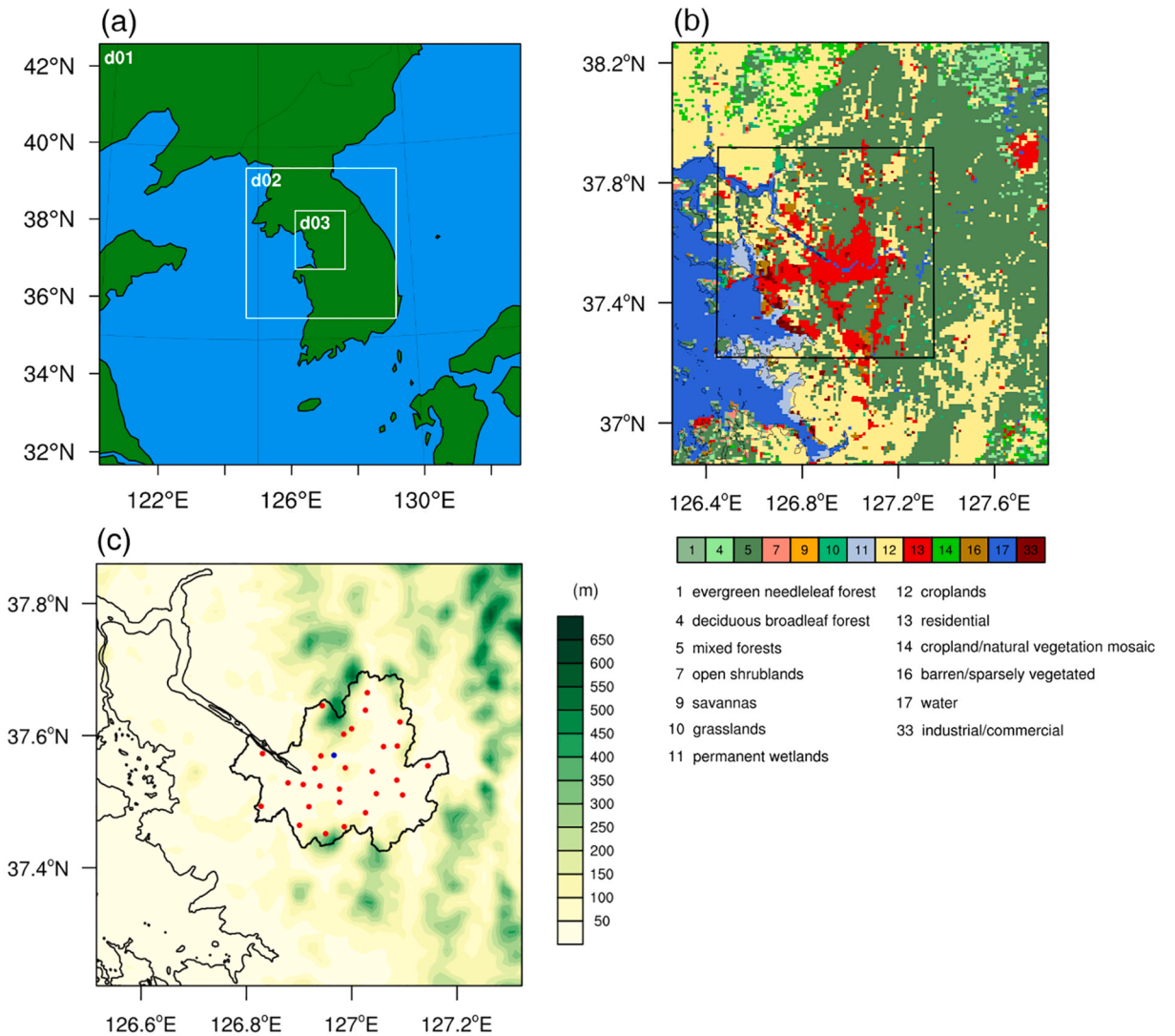


**Fig. 3.** (a) WRF model domain configuration, (b) land-use types in the innermost domain, and (c) topography of a subset of the innermost domain. The rectangle indicated by the black solid line in (b) is the domain of (c). In (c), the boundary of Seoul is contoured by the black solid line and the red and blue marks denote the locations of Automatic Weather Stations (AWSs) and Seoul meteorological observatory, respectively.

is 27.8 days, which is 3.4 times longer than that from 1979 to 2019 (8.1 days per a year). The heat wave duration in 2018 tends to be longer in inland regions than in coastal regions (Fig. 1a), and this is reflected in its anomaly distribution (Fig. 1e). The analyzed daily maximum temperature averaged over all the meteorological observatories in 2018 is 34.6 °C which is 0.7 °C higher than that from 1979 to 2019. Fig. 1 indicates that South Korea experienced longer-lasting and more intense heat wave in 2018. In fact, the 2018 heat wave is the longest-lasting heat wave on record in South Korea (KMA, 2018). For 2018, the analyzed daily maximum temperature averaged over the six largest cities in South Korea (Seoul, Incheon, Daejeon, Daegu, Gwangju, and Busan) is 35.2 °C and that averaged over all the observatories except the six largest cities is 34.5 °C, the difference being 0.7 °C. This suggests that the daytime urban heat island is combined with the heat wave, giving rise to higher air temperature in the largest cities.

Next, large-scale features associated with the 2018 heat wave are examined. For this, the monthly averaged fifth generation European Center for Medium-range Weather Forecasts (ECMWF) reanalysis (ERA5) data with a  $0.25^\circ \times 0.25^\circ$  horizontal resolution (Hersbach and Dick, 2016) are used. Fig. 2 shows the fields of 2-m temperature and 500- and 200-hPa geopotential heights averaged over July–August 2018 and their anomalies from July–August 1979–2019 climatology. 5880- and 12,480-m geopotential height isolines (Fig. 2c and e) are typically chosen to represent the horizontal extent of the North Pacific High and the Tibetan High, respectively (Choi et al., 2010; He et al., 2015; Ha et al., 2020). Positive 2-m temperature anomaly is prominent over the region between  $\sim 30^\circ\text{N}$  and  $\sim 45^\circ\text{N}$  which includes China, Korea, and Japan (Fig. 2b). The North Pacific High in 2018 is expanded farther northwestward and further intensified compared to the 1979–2019 climatology (Fig. 2c). Compared to the 1979–2019 climatology, the Tibetan High is also expanded farther and further intensified. The centers of large positive 500- and 200-hPa geopotential height anomaly regions are located northwest of the Korean Peninsula (Fig. 2d and f). The North Pacific High and Tibetan High expanded toward the Korean Peninsula and intensified are responsible for the heat wave South Korea experienced in 2018. These strong and persistent highs over the Korean Peninsula cause a sinking motion and make it difficult for hot air heated at the surface in the daytime to move farther upward. In other words, heat is trapped in the lower atmosphere. The sinking motion leads to clear skies and thus increases insolation and suppresses precipitation. Consequently, the near-surface air temperature is increased.

### 3. Model description and simulation setup

We use version 4.1.3 of the Weather Research and Forecasting (WRF) model (Skamarock et al., 2008) to examine cool-roof effects in Seoul during the 2018 heat wave. Three model domains with two-way nesting are considered with  $132 \times 132$ ,  $141 \times 141$ , and  $141 \times 165$  horizontal grids with sizes of 9, 3, and 1 km, respectively (Fig. 3a). The number of vertical layers is 72, and 38 vertical layers are located below the 2-km height. The physics parameterization schemes used are as follows: the WRF single-moment 6-class

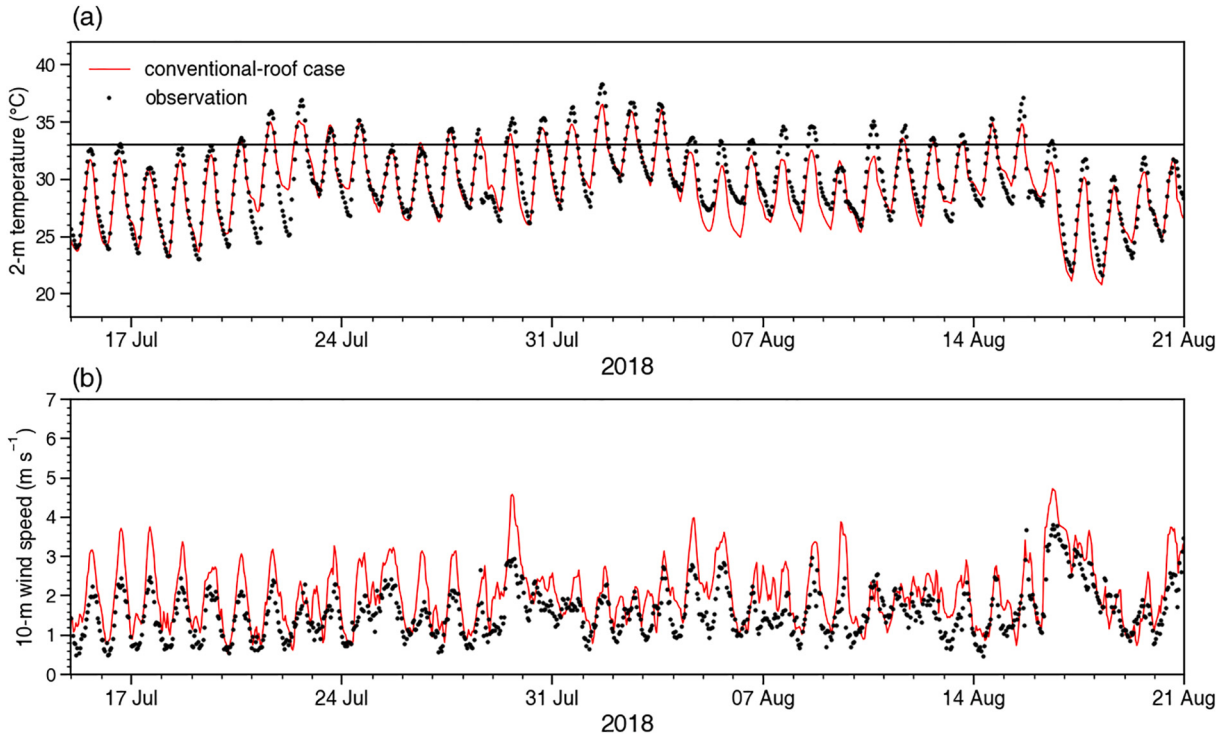


**Fig. 4.** Time series of (a) 2-m temperature and (b) 10-m wind speed in observations and the conventional-roof case. The observed 2-m temperature and 10-m wind speed are averaged over 28 AWSs (black dots), and the simulated ones are averaged over the same locations. The black solid line in (a) indicates 33 °C.

microphysics scheme (Hong and Lim, 2006), the Yonsei University planetary boundary layer scheme (Hong et al., 2006), the Kain–Fritsch convection scheme (Kain, 2004) which is applied only to the outermost domain, the Dudhia shortwave radiation scheme (Dudhia, 1989), the Rapid Radiative Transfer Model (RRTM) longwave radiation scheme (Mlawer et al., 1997), and the revised MM5 surface layer scheme (Jiménez et al., 2012). As an urban canopy model, the Seoul National University Urban Canopy Model (SNUUCM) (Ryu et al., 2011) coupled with the Noah land surface model (Chen and Dudhia, 2001) is employed. The SNUUCM is a single-layer urban canopy model that represents radiative energy transfer, conductive heat transfer, and turbulent energy and water exchanges occurring in urban canopies. Detailed descriptions on the SNUUCM are provided in Ryu et al. (2011). Two types of urban land-use categories are considered: the industrial/commercial and residential (Fig. 3b). In this study, the value of mean building height parameter is set to 30 m for the industrial/commercial and 22.5 m for the residential land-use types, referring to a report of Kim et al. (2019) that the grid-mean building height in Seoul at 1.5-km resolution reaches up to ~40 m in some highly developed areas.

Two simulations are conducted. One simulation has a roof albedo of 0.2, hereafter called the conventional-roof case. The other simulation has a roof albedo of 0.7, representing white roofs, and is hereafter called the cool-roof case. Note that roof albedo is controlled in the urban canopy model. The differences between the two simulations are regarded as cool-roof effects. The anthropogenic heat flux dataset with a horizontal resolution of 1 km is from Lee and Kim (2015), which is made by using an air pollutant emission database and a regression approach (Lee et al., 2014). For topography and land-use/land-cover (LULC) data, we follow Ryu and Baik (2013): the Shuttle Radar Topography Mission (SRTM) data with a 3-s (~90-m) horizontal resolution for topography and the Geographic Information System (GIS) data with a 4-m resolution for LULC. The ERA5 data with a horizontal grid resolution of 0.25° × 0.25° (Hersbach and Dick, 2016) are used as the initial and boundary conditions. The model is integrated from 2100 LST (UTC + 9 h) on 14 July 2018 to 0000 LST on 21 August 2018.

#### 4. Results and discussion

##### 4.1. Model validation

The model is validated against the observational data from 28 Automatic Weather Stations (AWSs) located within Seoul (Fig. 3c). Fig. 4 shows the time series of observed and simulated 2-m temperature and 10-m wind speed. The simulation is for the conventional-roof case. These are averages over the locations of the 28 AWSs. Overall, the simulated 2-m temperature closely follows the observed one and the diurnal variation of 2-m temperature is well simulated. In the diurnal cycles of 2-m temperature, however, the simulated maximum 2-m temperature is underestimated. The mean bias error (MBE) and root-mean-square-error (RMSE) are computed, which are defined as follows:

$$\text{MBE} = \frac{1}{N} \sum_{i=1}^N (S_i - O_i), \quad (1)$$

$$\text{RMSE} = \sqrt{\frac{1}{N} \sum_{i=1}^N (S_i - O_i)^2}, \quad (2)$$

where  $N$  is the number of data in the time series,  $S_i$  is the simulated value, and  $O_i$  is the observed value. The MBE and RMSE of 2-m temperature are  $-0.50\text{ }^\circ\text{C}$  and  $1.30\text{ }^\circ\text{C}$ , respectively, which are similar to those of previous studies (e.g., Hong et al., 2021). The simulated 10-m wind speed is overestimated, but its diurnal variation is well simulated. The MBE and RMSE of 10-m wind speed are  $0.47\text{ m s}^{-1}$  and  $0.67\text{ m s}^{-1}$ , respectively. The scatter plots of observed versus simulated 2-m temperature, 10-m wind speed, and 2-m water vapor mixing ratio (Fig. 5) exhibit underestimations of 2-m temperature and 2-m water vapor mixing ratio and an

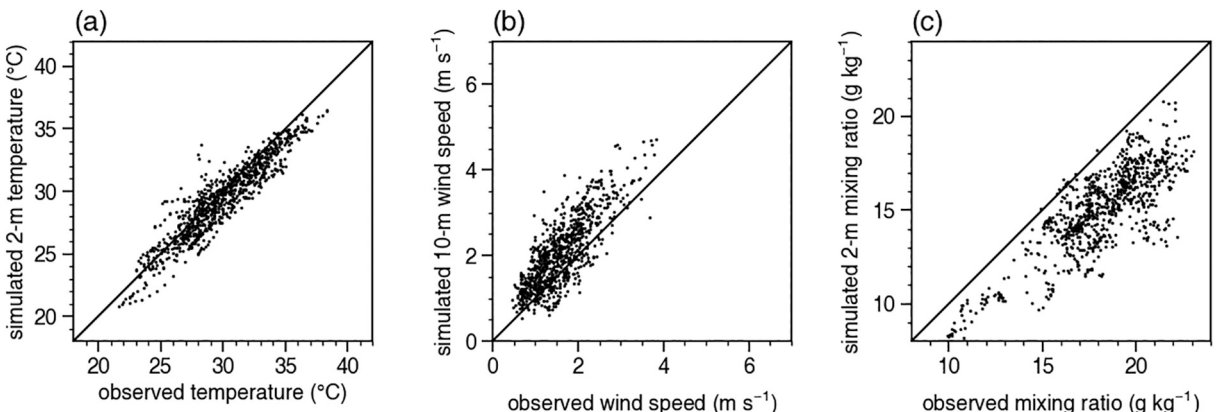


**Fig. 5.** Scatter plots of observed versus simulated (a) 2-m temperature, (b) 10-m wind speed, and (c) 2-m water vapor mixing ratio.

overestimation of 10-m wind speed. The 10-m wind speed is more overestimated for relatively higher wind speed range. The correlation coefficient between the observation and simulation is 0.93 for 2-m temperature, 0.81 for 10-m wind speed, and 0.84 for 2-m water vapor mixing ratio.

During the 2018 heat wave, the amount of electricity use increased greatly (KMA, 2018); thus, it is probable that anthropogenic heat emitted into the atmosphere increased substantially. If this were taken into account in the simulation, the cold bias (Fig. 5a) could be somewhat alleviated. A simple sensitivity run with all the model configurations same as those in the conventional-roof case but with anthropogenic heat flux doubled shows 2-m temperature increases of  $0.17^{\circ}\text{C}$  in 12–18 LST and  $0.38^{\circ}\text{C}$  in 00–06 LST (not shown). This suggests that the nighttime near-surface temperature can be greatly influenced by the change in anthropogenic heat emission during heat waves. It would be interesting in a future study to estimate anthropogenic heat flux on heat wave days and examine, through numerical model simulations, how much the near-surface air temperature increases with additional anthropogenic heat during the heat wave.

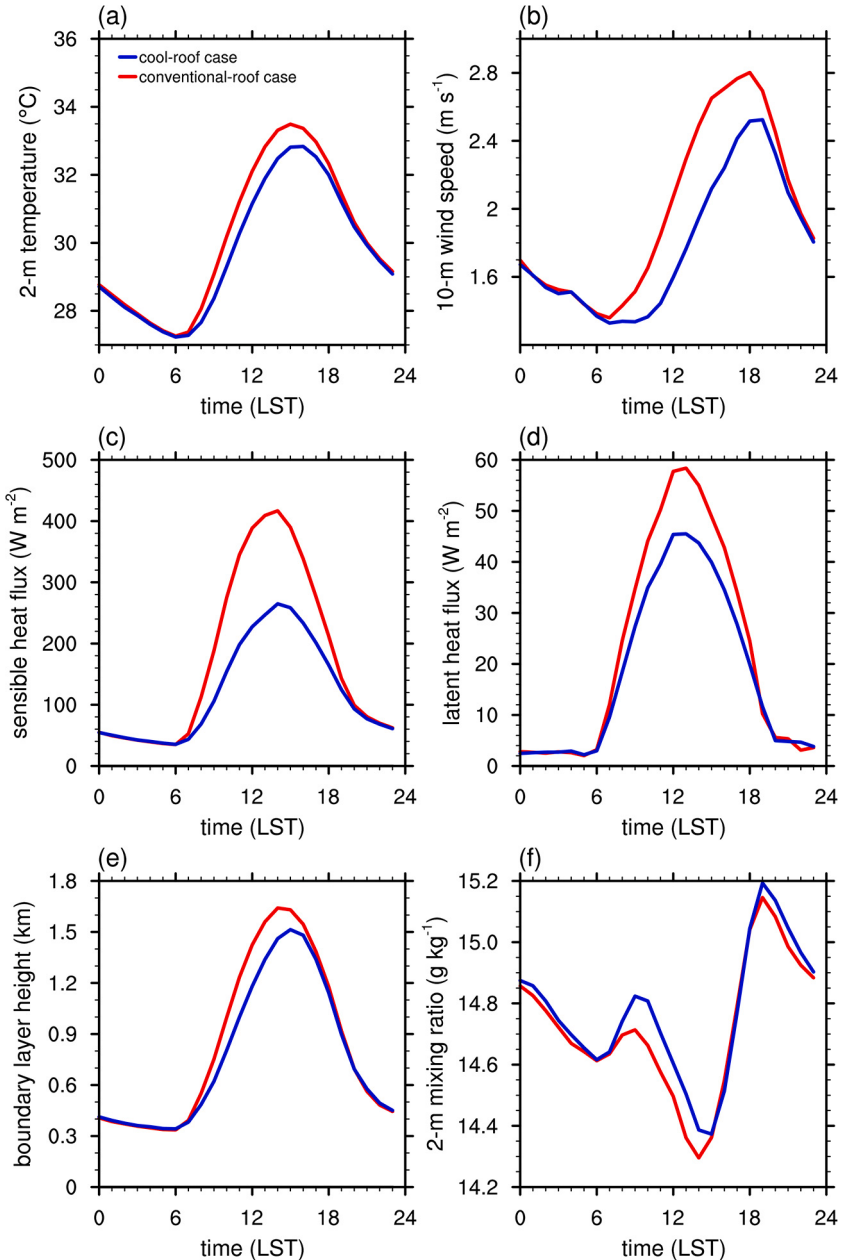


**Fig. 6.** Diurnal variations of (a) 2-m temperature, (b) 10-m wind speed, (c) surface sensible heat flux, (d) surface latent heat flux, (e) planetary boundary layer height, and (f) 2-m water vapor mixing ratio in the cool-roof and conventional-roof cases. These are averages for diurnal variations during the period from 15 July to 20 August 2018 and over the areas of Seoul belonging to the urban land-use category.

The systematic bias in the simulated wind speed is noticeable in Fig. 5b. From sensitivity experiments, it is found that the simulated 10-m wind speeds depend greatly on the choice of the values of building height parameters (not shown). This indicates that applying realistic building information data that substantially varies within Seoul to the simulation may reduce the bias, which deserves a future investigation. To further alleviate this bias, it may be needed to include realistic parameterizations that relates roughness parameters to the parameters of urban structure. This also deserves a future investigation. In spite of the deficiencies in the simulation, the 2-m temperature and 10-m wind speed, particularly their diurnal variations, are overall reasonably simulated (Figs. 4 and 5). This suggests that the simulation data can be used to investigate cool-roof effects that are revealed by differences between the cool-roof and conventional-roof cases.

#### 4.2. Cool-roof effects

In this subsection, we examine the effects of cool roofs on thermal and wind environments during the 2018 heat wave by comparing the cool-roof case with the conventional-roof case. Fig. 6 shows the diurnal variations of average 2-m temperature, 10-m wind speed, surface sensible and latent heat fluxes, planetary boundary layer height, and 2-m water vapor mixing ratio in the two cases. The time average is taken over the period from 15 July to 20 August 2018, and the spatial average is taken over the areas of Seoul belonging to the urban land-use category. It is seen from Fig. 6 that cool-roof effects are evident in the daytime but negligible or small in the nighttime. Since roof albedo is higher in the cool-roof case, incoming shortwave radiation is reflected more, resulting in a decrease in air temperature. The maximum decrease in 2-m temperature due to cool roofs is  $1.0^{\circ}\text{C}$  at 1200 LST. This value is similar to the average urban midday temperature reduction value ( $1.2^{\circ}\text{C}$ ) due to cool roofs in Guangzhou during heat wave events (Cao et al., 2015). The 10-m wind is consistently weaker in the cool-roof case than in the conventional-roof case, with a maximum decrease of  $0.5 \text{ m s}^{-1}$  at 1400 LST. The surface sensible heat flux is much larger than the surface latent heat flux in both the cases. Due to the decreased air temperature and wind speed in the cool-roof case, both the daytime surface sensible and latent heat fluxes are smaller in the cool-roof case than in the conventional-roof case. The maximum decrease is  $163 \text{ W m}^{-2}$  at 1300 LST in surface sensible heat flux and  $13 \text{ W m}^{-2}$  at 1300 LST in surface latent heat flux. The Bowen ratio, the ratio of the surface sensible heat flux to the surface latent heat flux, in the daytime is affected more by the decrease in the surface sensible heat flux than by the decrease in the surface latent heat flux, decreasing from 7.0 in the conventional-roof case to 5.4 in the cool-roof case at 1300 LST. The decreased surface sensible heat flux in the cool-roof case lowers the planetary boundary layer height, with a maximum decrease of 243 m at 1200 LST. Considering a close relation between the planetary boundary layer height and near-surface pollutant concentration (Wang et al., 2021), cool roofs can influence daytime

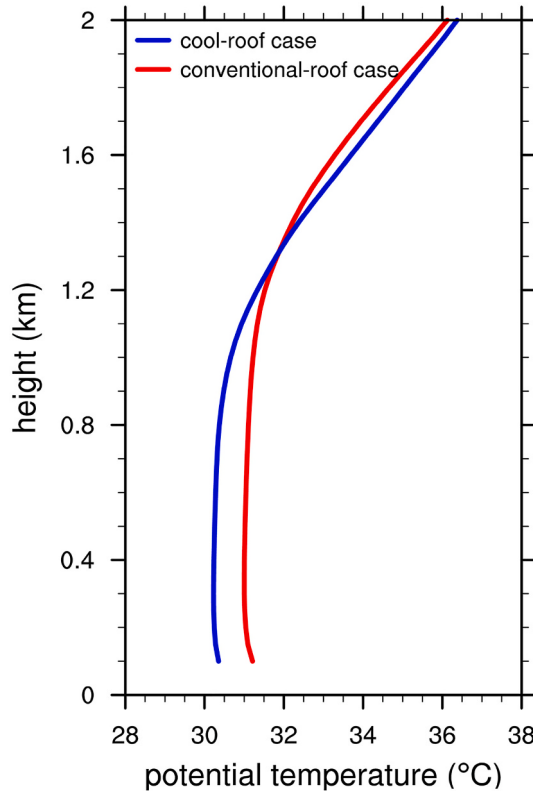


**Fig. 7.** Vertical profiles of potential temperature at 1200 LST in the cool-roof and conventional-roof cases. These are averages for 1200 LST during the period from 15 July to 20 August 2018 and over the areas of Seoul belonging to the urban land-use category.

near-surface air quality by lowering the daytime planetary boundary layer height. Also, the decrease in the planetary boundary layer height weakens the vertical mixing of water vapor, resulting in an increase in the daytime 2-m water vapor mixing ratio. The maximum increase in 2-m water vapor mixing ratio is  $0.14 \text{ g kg}^{-1}$  at 1000 LST. Due to the increase in 2-m water vapor mixing ratio and the decrease in 2-m temperature, the near-surface relative humidity in the cool-roof case increases (not shown).

To examine cool-roof effects on the structure of the planetary boundary layer, the vertical profiles of average potential temperature at 1200 LST in the cool-roof and conventional-roof cases are compared (Fig. 7). At 1200 LST, the planetary boundary layer height is 1181 m in the cool-roof case and 1424 m in the conventional-roof case. The nearly constant potential temperature layer is shallower in the cool-roof case than in the conventional-roof case. In the cool-roof case, the potential temperature below the 1.3-km height is lower compared to the conventional-roof case. Fig. 7 exhibits that the noticeable potential temperature decrease due to cool roofs appears in a deep layer in the planetary boundary layer. Chen and Zhang (2018) also reported similar results for the Suzhou–Wuxi–Changzhou metropolitan area. The average difference in potential temperature below the 1.2-km height (approximately the planetary boundary layer height in the cool-roof case) between the cool-roof and conventional-roof cases is  $0.7^\circ\text{C}$ .

The time series of average 2-m temperature in the cool-roof and conventional-roof cases and their differences are presented in Fig. 8. In the daily cycles of 2-m temperature, the decrease in daily maximum 2-m temperature is prominent and the change in daily minimum 2-m temperature is very small (Fig. 8a). The difference in 2-m temperature between the cool-roof and conventional-roof cases is mostly negative over the entire period (Fig. 8b). On 28 July, however, the 2-m temperature difference shows a positive peak. This day has the largest daily precipitation amount during the simulation period in both the cases. It is revealed that this positive peak is related to the differences in cloud development and precipitation between the two cases. On the occasion of the positive peak in 2-m temperature difference, the conventional-roof case produces noticeable amounts of convective clouds and precipitation, while the amounts are relatively small in the cool-roof case. Blocking of solar radiation and precipitation-induced near-surface cooling are stronger in the conventional-roof case. This results in the positive peak on that day.

The magnitude of cool-roof effects on urban air temperature fluctuates during the simulated heat-wave period. Fig. 9a shows the relationship between the heat wave intensity represented by the daily maximum 2-m temperature in the conventional-roof case and the cool-roof effects on the daily maximum 2-m temperature. To keep out the complicated effects of clouds and precipitation, 9 days when the daily precipitation amount is larger than 0.1 mm in either the conventional-roof case or the cool-roof case are excluded when calculating the linear regression fit and correlation coefficient. A statistically significant negative correlation ( $R = -0.40$ ) is found, indicating that the cool-roof effect on near-surface temperature is reduced as the heat wave intensifies. The linear regression shows that when the daily maximum temperature in the conventional-roof case increases from 30 to  $35^\circ\text{C}$ , the cool-roof effect on the daily maximum temperature decreases by 21%. This result does not agree with what is commonly expected, that is, the cool-roof effect is more pronounced for extreme heat waves (e.g., Cao et al., 2015). The daily maximum temperature in the conventional-roof case has a

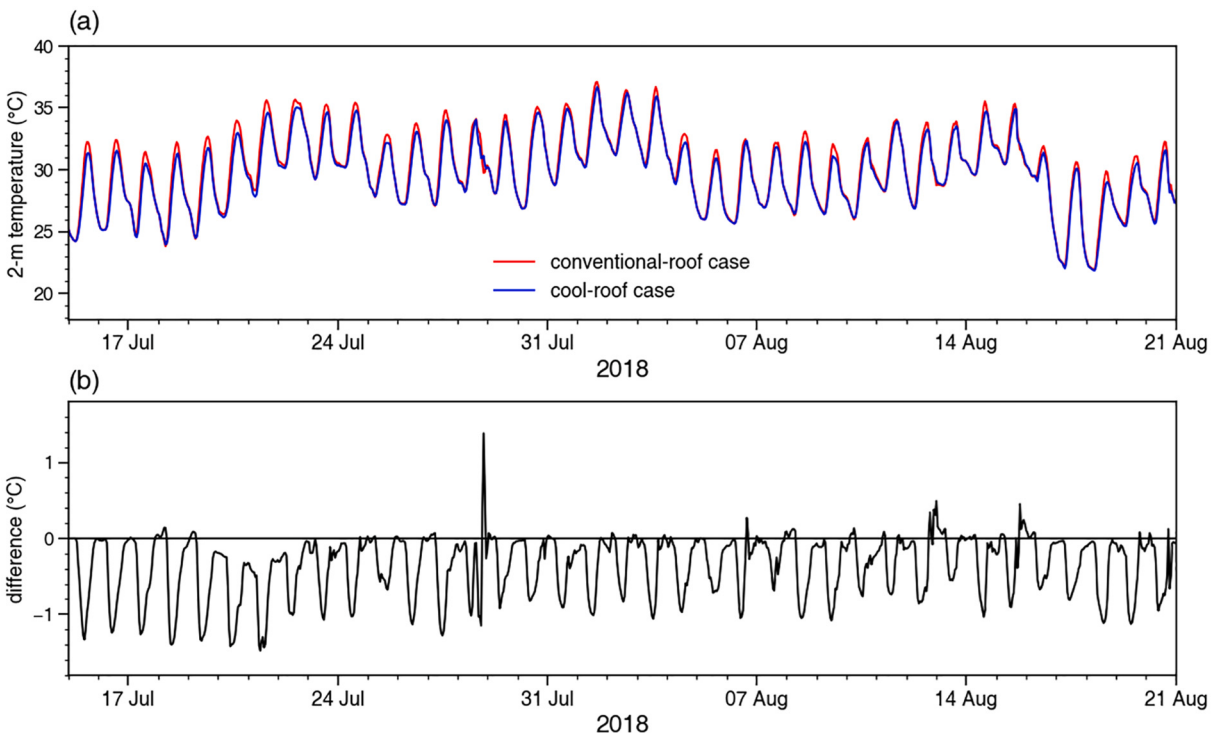


**Fig. 8.** (a) Time series of 2-m temperature averaged over the areas of Seoul belonging to the urban land-use category in the cool-roof and conventional-roof cases. (b) Differences between the two cases (the cool-roof case minus the conventional-roof case).

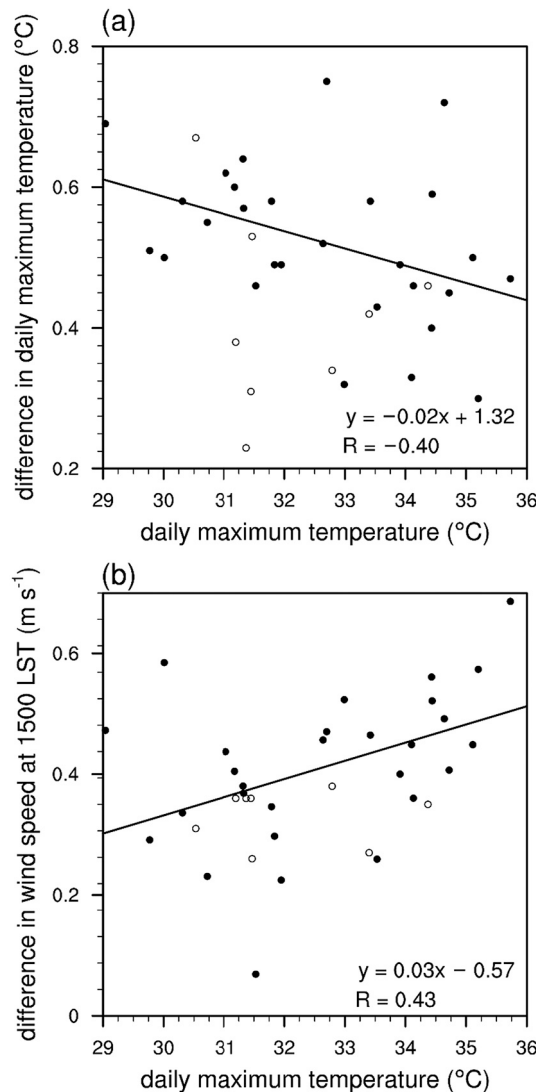


**Fig. 9.** Scatter plots of the daily maximum 2-m temperature in the conventional-roof case versus (a) difference in daily maximum temperature and (b) difference in 1500-LST wind speed between the cool-roof case and conventional-roof case (the cool-roof case minus the conventional-roof case). Days when the daily precipitation amount is larger than 0.1 mm in either the cool-roof case or conventional-roof case are marked with hollow circles and are excluded when calculating the linear regression fit and correlation coefficient. The rest of the days are marked with filled circles. The obtained linear regression fit and correlation coefficient are statistically significant ( $p < 0.05$ ).

statistically significant positive correlation ( $R = 0.43$ ) with the cool-roof effect on near-surface wind speed at 1500 LST (Fig. 9b). Cool roofs reduce near-surface wind speed, and this cool-roof effect is enhanced as the heat wave intensifies. The difference in near-surface wind speed represents the cool roof-induced changes in local winds such as urban breeze and sea breeze in the daytime, which can bring the outside cool air into the city. Therefore, the greater cool-roof effect on near-surface wind for high heat wave intensity may have led to the weakening of cool-roof effect on urban air temperature.

Fig. 10 shows average 2-m temperature and 10-m wind vector fields at 1200 LST in the cool-roof and conventional-roof cases and their differences. Large differences in 2-m temperature between the two cases are seen in Seoul and urbanized regions around Seoul (Figs. 3b and 10). The urban areas within Seoul exhibits a decrease in 2-m temperature by  $1.0 ^{\circ}\text{C}$  on average as a consequence of having cool roofs. Notice that Incheon is located west of Seoul and the 2-m temperature decrease in Incheon due to cool roofs is similar, in its magnitude, to that in Seoul. It is interesting to observe that the cooling due to cool roofs is widespread in the areas outside Seoul (Fig. 10c). Even in the regions where the land-use type is not in the urban category and therefore no changes in albedo are applied, the cool-roof effect on temperature is detected although the 2-m temperature decrease is small. At 1200 LST, sea breeze appears over the sea and penetrates into the coastal land region. In the cool-roof case, the near-surface temperature, thus the near-surface land-sea temperature difference, decreases. Accordingly, sea breeze is weaker in the cool-roof case than in the conventional-roof case (Fig. 10a and b). The 10-m zonal wind component averaged along Line A in Fig. 10a that roughly represents the intensity of sea breeze blowing

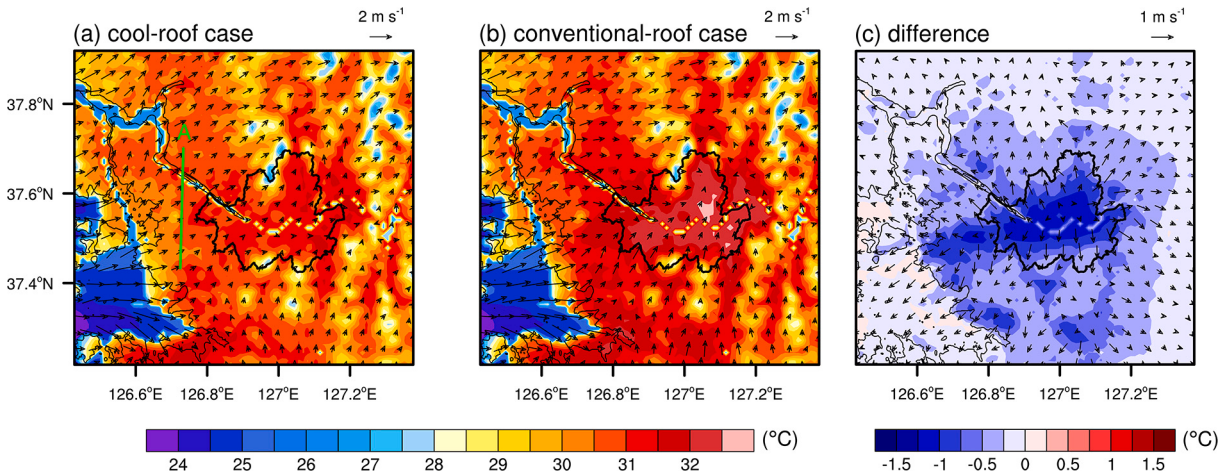


**Fig. 10.** 2-m temperature and 10-m wind vector fields at 1200 LST. These are averages for 1200 LST during the period from 15 July to 20 August 2018 in the (a) cool-roof case and (b) conventional-roof case. (c) Differences in 2-m temperature and 10-m wind vector between the two cases (the cool-roof case minus the conventional-roof case). Line A in (a) indicates the line along which the 10-m zonal wind component is averaged to roughly represent the intensity of sea breeze blowing toward Seoul.

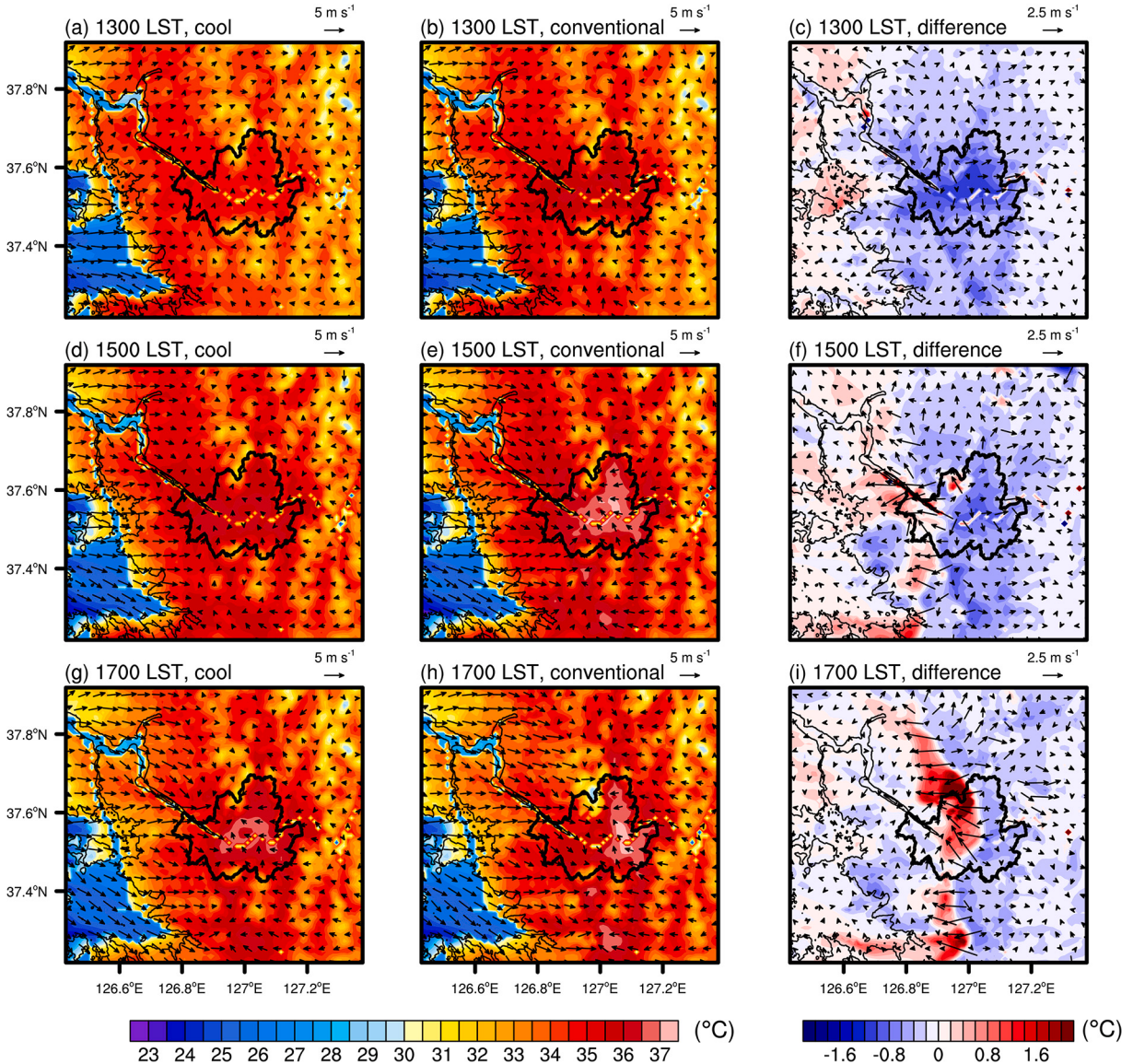
toward Seoul is 10% smaller in the cool-roof case ( $1.71 \text{ m s}^{-1}$ ) than in the conventional-roof case ( $1.91 \text{ m s}^{-1}$ ). Due to the cooling, the near-surface wind in Seoul is diverging toward the outside (Fig. 10c). This diverging wind acts to weaken the urban breeze toward Seoul from its surroundings.

Fig. 10 shows composite temperature and wind vector fields obtained by averaging simulation data for 1200 LST from 15 July to 20 August 2018, which reveals the cool-roof effects at this time during the heat wave. Summertime wind fields in Seoul and the surrounding regions under clear skies and weak synoptic winds are spatially and temporally complex. In the daytime, interactions among urban breeze, sea breeze, and valley wind take place in these areas (Ryu and Baik, 2013). These local winds and their interactions may reveal interesting features regarding cool-roof effects. Here, we present such interesting features that appear on 2 August 2018 in the cool-roof and conventional-roof cases.

The fields of 2-m temperature and 10-m wind vector at 1300, 1500, and 1700 LST on 2 August 2018 in the cool-roof and conventional-roof cases together with their differences are shown in Fig. 11. At 1300 LST, the decrease in 2-m temperature due to cool roofs is evident in the entire Seoul. The maximum decrease in 2-m temperature in Seoul is  $1.2^\circ\text{C}$ . Sea breeze is well established over the sea and in the coastal region in both the cases. In the conventional-roof case, the urban breeze is clearly seen. The diverging wind due to the cooling effect of cool roofs (Fig. 11c) weakens the urban breeze, masking the urban breeze signal in the wind field (Fig. 11a). At 1500 LST, the maximum 2-m temperature in Seoul is as high as  $37.1^\circ\text{C}$  in the conventional-roof case, which is  $0.6^\circ\text{C}$  higher than that in the cool-roof case. The sea breeze penetrates farther into the inland in both the cases. The sea breeze intensities (along Line A in Fig. 10a as defined above) at 1300 LST and 1500 LST are both 8% smaller in the cool-roof case than in the conventional-roof case. In the conventional-roof case, the urban breeze is stronger at 1500 LST than at 1300 LST, and in the western part of Seoul, the urban breeze constructively interacts with the sea breeze. In the cool-roof case, on the other hand, the sea breeze does not reach Seoul yet and the urban breeze is masked because of the diverging wind (Fig. 11d and f). At 1700 LST, the sea breeze penetrates into the inland farther in the conventional-roof case, similar to the situations in the cool-roof case like at 1300 and 1500 LST. At 1700 LST, the sea breeze reaches the eastern part of Seoul in the conventional-roof case but it reaches the western part of Seoul in the cool-roof case. Despite cool roofs being considered, there appears a prominent region of noticeable positive temperature difference which extends approximately in the north–south direction with the maximum difference in Seoul being  $3.5^\circ\text{C}$  (Fig. 11i). The sea breeze brings cool air to the land. At 1700 LST, the region of noticeable positive temperature difference experiences sea breeze in the conventional-roof case but not so much in the cool-roof case. This sea-breeze effect contributes to the cooling in the region in the conventional-roof case. In the region of noticeable positive temperature difference, the cooling caused by the sea breeze in the conventional-roof case is dominant over the cooling due to cool roofs in the cool-roof case.

This peculiar warming over some areas in Seoul due to cool roofs does not occur every day. The stronger cooling by the sea breeze in the conventional-roof case is repeatedly seen on many days, but it is often not enough to overcome the stronger cooling in Seoul due to cool roofs in the cool-roof case. Complex interactions among local winds make it difficult to find out favorable conditions for this phenomenon, and this deserves further investigation.

In this study, the prominent effects of cool roofs that decrease near-surface air temperature are found. At the same time, however, cool roofs result in an increase in near-surface relative humidity due to the weakening of vertical mixing and the decrease in saturation water vapor pressure, which can lead to uncomfortable conditions due to the reduced evaporation of sweat that helps with lowering the body temperature. To find out the effects of cool roofs on thermal comfort of human body, three thermal comfort indices that consider both air temperature and humidity are calculated: the heat index of Rothfusz (1990) derived from the apparent temperature of Steadman (1979), the temperature-humidity index (discomfort index) of Thom (1959), and the humidity index of Masterton and



**Fig. 11.** 2-m temperature and 10-m wind vector fields at (a, b) 1300, (d, e) 1500, and (g, h) 1700 LST in the cool-roof case (first column) and conventional-roof case (second column) on 2 August 2018. (c), (f), and (i) (third column) are differences between the two cases (the cool-roof case minus the conventional-roof case) at respective times.

**Table 1**

Formulas of three thermal comfort indices, their maximum values in the conventional-roof and cool-roof cases, and their maximum decreases due to cool roofs. Here,  $T$  is the dry-bulb temperature (°C),  $H$  is the relative humidity (%),  $p_v$  is the atmospheric water vapor pressure (hPa). Values of  $c_1$ ,  $c_2$ , ...  $c_9$  are  $-8.7847$ ,  $1.6114$ ,  $2.3385$ ,  $-0.14612$ ,  $-1.2308 \times 10^{-2}$ ,  $-1.6425 \times 10^{-2}$ ,  $2.2117 \times 10^{-3}$ ,  $7.2546 \times 10^{-4}$ , and  $-3.582 \times 10^{-6}$ . The formulas used to calculate these indices follow Coccoccio et al. (2016).

	Thermal comfort indices		
	Heat index (Rothfusz, 1990)	Temperature-humidity index (Thom, 1959)	Humidex index (Masterton and Richardson, 1979)
Formula	$c_1 + c_2 T + c_3 H + c_4 TH + c_5 T^2 + c_6 H^2 + c_7 T^2 H + c_8 TH^2 + c_9 T^2 H^2$	$T - 0.55(1 - 0.01H) \times (T - 14.5)$	$T + \frac{5}{9}(p_v - 10)$
Maximum (conventional-roof case)	$35.8^\circ\text{C}$	$27.6^\circ\text{C}$	$40.8^\circ\text{C}$
Maximum (cool-roof case)	$35.2^\circ\text{C}$	$27.4^\circ\text{C}$	$40.3^\circ\text{C}$
Maximum decrease	$1.0^\circ\text{C}$	$0.4^\circ\text{C}$	$0.9^\circ\text{C}$

**Richardson (1979).** The formulas used to calculate these indices follow Coccoco et al. (2016). Table 1 shows the formulas for the indices and the maximum decreases in the indices due to cool roofs. All three indices decrease due to cool roofs showing maximum decreases of 1.0 °C, 0.4 °C, and 0.9 °C, respectively, at 1200 LST. This indicates that the change in thermal comfort due to cool roofs is dominated by the decrease in near-surface air temperature. The increase in near-surface relative humidity induced by cool roofs, which maximizes at 3.6 percentage points, to some extent dilutes the improvement in thermal comfort made by the cool-roof induced decrease in near-surface air temperature, but its role is minor. This shows that cool roofs are an effective strategy for promoting human health and comfort in urban areas.

## 5. Summary and conclusions

Cool-roof effects on thermal and wind environments in Seoul during the 2018 heat wave were examined using the WRF model. In the cool-roof case, the 2-m temperature, 10-m wind speed, surface sensible and latent heat fluxes, and planetary boundary layer height averaged over the urban areas within Seoul all decrease but the 2-m water vapor mixing ratio increases in the daytime. The daytime maximum decreases are 1.0 °C in 2-m temperature, 0.5 m s<sup>-1</sup> in 10-m wind speed, 163 W m<sup>-2</sup> in surface sensible heat flux, 13 W m<sup>-2</sup> in surface latent heat flux, and 243 m in planetary boundary layer height. The daytime maximum increase in water vapor mixing ratio is 0.14 g kg<sup>-1</sup>. The decrease in near-surface temperature acts to weaken urban breeze and sea breeze. It was found that on occasion the cool-roof case leads to higher near-surface air temperature at late afternoon times in a region of Seoul compared to the conventional-roof case. This feature can appear when the cooling caused by the sea breeze in the conventional-roof case is dominant over the cooling due to cool roofs in the cool-roof case. This is one of the important results in this study because it shows that on occasion the changes in local winds induced by cool roofs can actually reverse the cool-roof effects on temperature, acting against the intention of building cool roofs.

The magnitude of cool-roof effects on near-surface temperature in Seoul during heat waves can differ depending on the intensity of heat waves. This study shows that the near-surface temperature reduction due to cool roofs tends to decrease with increasing heat wave intensity. From the linear regression analysis, it is expected that the cool-roof effect on the daily maximum temperature would decrease by 21% if the daily maximum temperature in the conventional-roof case increases from 30 to 35 °C. This is a noteworthy feature because the cool-roof effect is known to be more pronounced for extreme heat waves (e.g., Cao et al., 2015). Local winds in Seoul and their interactions with heat wave intensity seem to play some role in this interesting feature. A further systematic study of this relationship and associated mechanisms considering various conditions related to local winds is therefore needed. It would be challenging to investigate the interactions of urban heat islands with heat waves in the presence of interacting local winds through well-designed numerical simulations with cool and conventional roofs. This study also shows that the largest cities experienced higher near-surface air temperature than other regions during the 2018 heat wave. The responses of the largest cities and other regions to heat waves may be different, and this also deserves a further investigation.

## Declaration of Competing Interest

The authors declare that they have no known competing financial interests or personal relationships that could have appeared to influence the work reported in this paper.

## Acknowledgements

The authors are grateful to anonymous reviewers for providing valuable comments on this work. This work was funded by the Korea Meteorological Administration Research and Development Program “Advanced Research on Aviation Meteorology and Urban Meteorology” under Grant (KMA2018-00621).

## References

- Balany, F., Ng, A.W.M., Muttill, N., Muthukumaran, S., Wong, M.S., 2020. Green infrastructures as an urban heat island mitigation strategy—a review. *Water* 12, 3577.
- Barriopedro, D., Fischer, E.M., Luterbacher, J., Trigo, R.M., García-Herrera, R., 2011. The hot summer of 2010: redrawing the temperature record map of Europe. *Science* 332, 220–224.
- Cao, M., Rosado, P., Lin, Z., Levinson, R., Millstein, D., 2015. Cool roofs in Guangzhou, China: outdoor air temperature reductions during heat waves and typical summer conditions. *Environ. Sci. Technol.* 49, 14672–14679.
- Chen, F., Dudhia, J., 2001. Coupling an advanced land surface-hydrology model with the Penn State-NCAR MM5 modeling system. Part I: model implementation and sensitivity. *Mon. Weather Rev.* 129, 569–585.
- Chen, Y., Zhang, N., 2018. Urban heat island mitigation effectiveness under extreme heat conditions in the Suzhou-Wuxi-Changzhou metropolitan area, China. *J. Appl. Meteorol. Climatol.* 57, 235–253.
- Choi, K.-S., Kim, D.-W., Byun, H.-R., 2010. Statistical model for seasonal prediction of tropical cyclone frequency in the mid-latitudes of East Asia. *Theor. Appl. Climatol.* 102, 105–114.
- Coccoco, S., Kämpf, J., Scartezzini, J.-L., Pearlmuter, D., 2016. Outdoor human comfort and thermal stress: a comprehensive review on models and standards. *Urban Clim.* 18, 33–57.
- Coutts, A.M., Daly, E., Beringer, J., Tapper, N.J., 2013. Assessing practical measures to reduce urban heat: green and cool roofs. *Build. Environ.* 70, 266–276.
- Cowan, T., Purich, A., Perkins, S., Pezza, A., Boschat, G., Sadler, K., 2014. More frequent, longer, and hotter heat waves for Australia in the twenty-first century. *J. Clim.* 27, 5851–5871.
- Dudhia, J., 1989. Numerical study of convection observed during the Winter Monsoon Experiment using a mesoscale two-dimensional model. *J. Atmos. Sci.* 46, 3077–3107.

- Easterling, D.R., Evans, J.L., Groisman, P.Y., Karl, T.R., Kunkel, K.E., Ambenje, P., 2000. Observed variability and trends in extreme climate events: a brief review. *Bull. Am. Meteorol. Soc.* 81, 417–426.
- Geer, I.W., 1996. Glossary of Weather and Climate. American Meteorological Society.
- Ha, K.-J., Yeo, J.-H., Seo, Y.-W., Chung, E.-S., Moon, J.-Y., Feng, X., Lee, Y.-W., Ho, C.-H., 2020. What caused the extraordinarily hot 2018 summer in Korea? *J. Meteorol. Soc. Jpn.* 98, 153–167.
- Han, B.-S., Baik, J.-J., Kwak, K.-H., Park, S.-B., 2020. Effects of cool roofs on turbulent coherent structures and ozone air quality in Seoul. *Atmos. Environ.* 117476.
- He, C., Zhou, T., Lin, A., Wu, B., Gu, D., Li, C., Zheng, B., 2015. Enhanced or weakened western North Pacific subtropical high under global warming? *Sci. Rep.* 5, 16771.
- Hersbach, H., Dick, D., 2016. ERA5 reanalysis is in production. *ECMWF Newsletter* 147, 7.
- Hong, S.-O., Byon, J.-Y., Kim, D.-H., Lee, S.-S., Kim, Y.-H., 2021. Effects of land cover change on summer urban heat island intensity and latent heat index in Seoul metropolitan area, Korea. *Atmosphere* 31, 143–156 (in Korean with English abstract).
- Hong, S.-Y., Lim, J.-O.J., 2006. The WRF single-moment 6-class microphysics scheme (WSM6). *J. Korean Meteorol. Soc.* 42, 129–151.
- Hong, S.-Y., Noh, Y., Dudhia, J., 2006. A new vertical diffusion package with an explicit treatment of entrainment processes. *Mon. Weather Rev.* 134, 2318–2341.
- Imran, H.M., Kala, J., Ng, A.W.M., Muthukumaran, S., 2018. Effectiveness of green and cool roofs in mitigating urban heat island effects during a heatwave event in the city of Melbourne in southeast Australia. *J. Clean. Prod.* 197, 393–405.
- Jiménez, P.A., Dudhia, J., González-Rouco, J.F., Navarro, J., Montávez, J.P., García-Bustamante, E., 2012. A revised scheme for the WRF surface layer formulation. *Mon. Weather Rev.* 140, 898–918.
- Kain, J.S., 2004. The Kain–Fritsch convective parameterization: an update. *J. Appl. Meteorol.* 43, 170–181.
- Kim, D.-H., Hong, S.-O., Byon, J.-Y., Park, H., Ha, J.-C., 2019. Development and evaluation of urban canopy model based on Unified Model input data using urban building information data in Seoul. *Atmosphere* 29, 417–427 (in Korean with English abstract).
- KMA, 2018. Abnormal Climate Report, Korea Meteorological Administration (in Korean).
- Kovats, R.S., Hajat, S., 2008. Heat stress and public health: a critical review. *Annu. Rev. Public Health* 29, 41–55.
- Lee, H.-D., Min, K.-H., Bae, J.-H., Cha, D.-H., 2020. Characteristics and comparison of 2016 and 2018 heat wave in Korea. *Atmosphere* 30, 1–15 (in Korean with English abstract).
- Lee, S.-H., Kim, S.-T., 2015. Estimation of anthropogenic heat emission over South Korea using a statistical regression method. *Asia-Pac. J. Atmos. Sci.* 51, 157–166.
- Lee, S.-H., McKeen, S.A., Sailor, D.J., 2014. A regression approach for estimation of anthropogenic heat flux based on a bottom-up air pollutant emission database. *Atmos. Environ.* 95, 629–633.
- Li, D., Bou-Zeid, E., 2013. Synergistic interactions between urban heat islands and heat waves: the impact in cities is larger than the sum of its parts. *J. Appl. Meteorol. Climatol.* 52, 2051–2064.
- Masterton, J., Richardson, F.A., 1979. Humidex: A Method of Quantifying Human Discomfort Due to Excessive Heat and Humidity. Environment Canada, Downsview, Ontario, Canada.
- Meehl, G.A., Tebaldi, C., 2004. More intense, more frequent, and longer lasting heat waves in the 21st century. *Science* 305, 994–997.
- Mlawer, E.J., Taubman, S.J., Brown, P.D., Iacono, M.J., Clough, S.A., 1997. Radiative transfer for inhomogeneous atmospheres: RRTM, a validated correlated-k model for the longwave. *J. Geophys. Res. Atmos.* 102, 16663–16682.
- Oleson, K.W., Bonan, G.B., Feddema, J., 2010. Effects of white roofs on urban temperature in a global model. *Geophys. Res. Lett.* 37, L03701.
- Rothfusz, L.P., 1990. The Heat Index Equation (or, more than you ever wanted to know about heat index). National Oceanic and Atmospheric Administration, National Weather Service, Office of Meteorology, Fort Worth, Texas.
- Ryu, Y.-H., Baik, J.-J., 2013. Daytime local circulations and their interactions in the Seoul metropolitan area. *J. Appl. Meteorol. Climatol.* 52, 784–801.
- Ryu, Y.-H., Baik, J.-J., Lee, S.-H., 2011. A new single-layer urban canopy model for use in mesoscale atmospheric models. *J. Appl. Meteorol. Climatol.* 50, 1773–1794.
- Santamouris, M., 2014. Cooling the cities – a review of reflective and green roof mitigation technologies to fight heat island and improve comfort in urban environments. *Sol. Energy* 103, 682–703.
- Sharma, A., Conry, P., Fernando, H.J.S., Hamlet, A.F., Hellmann, J.J., Chen, F., 2016. Green and cool roofs to mitigate urban heat island effects in the Chicago metropolitan area: evaluation with a regional climate model. *Environ. Res. Lett.* 11, 064004.
- Skamarock, W.C., Klemp, J., Dudhia, J., Gill, D.O., Barker, D.M., Duda, M.G., Huang, X.-Y., Wang, W., Powers, J.G., 2008. A description of the Advanced Research WRF version 3. NCAR Tech. Note TN-475+STR.
- Steadman, R.G., 1979. The assessment of sultriness. Part I: a temperature-humidity index based on human physiology and clothing science. *J. Appl. Meteorol. Climatol.* 18, 861–873.
- Taleghani, M., 2018. Outdoor thermal comfort by different heat mitigation strategies- a review. *Renew. Sust. Energ. Rev.* 81, 2011–2018.
- Thom, E.C., 1959. The discomfort index. *Weatherwise* 12, 57–61.
- Wang, M., Tang, G., Liu, Y., Ma, M., Yu, M., Hu, B., Zhang, Y., Wang, Y., Wang, Y., 2021. The difference in the boundary layer height between urban and suburban areas in Beijing and its implications for air pollution. *Atmos. Environ.* 260, 118552.